AAPT PHYSICS EDUCATION | AMERICAN JOURNAL of PHYSICS

Mie scattering

R. M. Drake and J. E. Gordon

Citation: American Journal of Physics **53**, 955 (1985); doi: 10.1119/1.14011
View online: http://dx.doi.org/10.1119/1.14011
View Table of Contents: http://scitation.aip.org/content/aapt/journal/ajp/53/10?ver=pdfcov
Published by the American Association of Physics Teachers

tions. How much easier it is to say that a body moving at constant velocity relative to an inertial frame by definition experiences no (net) force.

V. CONCLUSION

Whether or not a frame is grossly noninertial is obvious to us without recourse to impossibly precise measures of time. In the rigid noninertial frame ostensibly free bodies possess the same acceleration, given the same position and velocity. Clearly, the practical test of inertiality is found in the motion of apparently free bodies, even though we may not be absolutely certain that the bodies are indeed free.

Yet the nagging question remains: Why is it that in frames in which fixed clocks do not keep time at the same rate, free bodies spontaneously accelerate? We have no answer. Yet lacking an answer does not preclude our using the properties of space-time to identify the inertial frame and through that identification to avoid the embarrassing pitfalls into which we stumble when we attempt to approach inertiality using forces.

[1]For an excellent discussion of the logical inconsistencies in Newton's laws of motion, see L. Eisenbud, Am. J. Phys. **26,** 144 (1958).

[2]Eddington's famous parody of Newton's first law comes to mind: "Every body continues in a state of rest or of uniform motion in a right line except insofar as it doesn't;" A. S. Eddington, *The Nature of the Physical World* (Macmillan, New York, 1929).

[3]In the relativistic domain more than one definition of force is used: There is the coordinate force defined to be $d\mathbf{p}/dt$, where $d\mathbf{p}$ is the change in the momentum of a body occurring during the lapse of coordinate time dt; there is the relativistic force defined to be $d\mathbf{p}/d\tau$, where $d\tau$ is the corresponding lapse of proper time on the body.

[4]If, relative to an inertial frame, the acceleration of a rigid frame is rectilinear, the spatial geometry of the accelerated frame is Euclidean.

[5]See R. Brehme, Am. J. Phys. **53,** 56 (1985), and H. Erlichson, Am. J. Phys. **53,** 53 (1985), for differing points of view on the synchronization of distant clocks.

[6]This discussion is suggested by a method proposed by Marion and Hornyak; J. Marion and W. Hornyak, *Principles of Physics* (Saunders, New York, 1984), pp. 69–74.

Mie scattering[a)]

R. M. Drake
Department of Physics, University of California, Santa Barbara, California 93106

J. E. Gordon
Department of Physics, Amherst College, Amherst, Massachusetts 01002

(Received 22 May 1984; accepted for publication 17 October 1984)

We describe a light scattering apparatus in which the detection electronics are interfaced to a microcomputer. We report experimental results obtained with the apparatus on the scattering of 0.6328-μm laser light from dilute water suspensions of polystyrene latex spheres with diameters of 2 and 5 μm. Experimental results are compared with theoretical scattering curves obtained from a simple, yet reasonably good, approximation of Mie scattering theory.

I. INTRODUCTION

Scientists have long been intrigued with the problem of light scattered from small particles. Such marvels as the blue sky, the orange sunset, and white clouds delight the eye of all observers, scientific or not. However, for physicists from the 19th century onward, the central explanation for these and related phenomena has clearly resided in the solution of an apparently simple boundary value problem—the scattering of plane waves by a small sphere. As is well known, a solution of this problem for the case in which the sphere's diameter is much less than the wavelength λ was first obtained by Rayleigh.[1,2] The name most often associated with the scattering problem when the sphere's diameter is not much smaller than λ is that of Gustave Mie,[3] although it has been pointed out[4,5] that some of the most eminent 19th and early 20th century mathematical physicists also worked on the problem.

While Mie scattering is a conceptually simple boundary value problem—it is necessary "only" to solve Maxwell's equations and the associated boundary conditions—the actual obtaining of the solution is a formidable algebraic task. No less formidable is the chore of extracting from the formal Mie solution the angular dependence of the scattered radiation or the way in which this scattered radiation depends upon particle size and index of refraction. Tabulations of the scattering results are available for given values of m (relative index of refraction) and $ka(k = 2\pi/\lambda, a =$ radius of the sphere) but these tabulations often are for only a few values of ka[6] or for angular intervals of 5° or 10°.[7] The tables of Chu *et al.*[8] permit a calculation of the scattered intensity at any arbitrary angle for a range of m and ka values. Especially for large ka, however, this calculation is tedious (although it provides a nice exercise in computer

programming) and offers little physical insight into how the angular positions of the relative maxima and minima in the angular dependence of the scattering depend upon m and ka.

With the coming of the inexpensive helium–neon laser, observations of Mie scattering constitute a feasible addition to an advanced undergraduate laboratory. The value of such an addition is, in our view, much enhanced if the experimental data can be compared with theoretical predictions which undergraduates can themselves carry out. Therefore, in what follows, we present a model for Mie scattering which, although crude, allows a simple means of approximating the dependence of scattered intensity upon angle. We then describe an experimental arrangement for observing Mie scattering, and, finally, compare experimental and theoretical results for the case of scattering of the 0.6328-μm He–Ne line by 2- and 5-μm-diam latex spheres.

II. THEORY

Let us examine the problem of plane electromagnetic wave scattering by a dielectric sphere, not by solving Maxwell's equations plus boundary conditions, that is, not á la Mie, but rather by looking at the integral formulation of the problem.[4] In Fig. 1 we depict a plane wave incident upon a small sphere of radius a. We shall assume the sphere to be homogeneous, nonmagnetic, and to have a real relative index of refraction m. We shall further assume that the incident wave is linearly polarized, and that the scattered radiation is to be observed in a plane perpendicular to this direction of polarization and at distances from the sphere, which are $\gg a$. In the integral formulation (the spatial part of) the *scattered* electric field outside the sphere, $\mathbf{E}_s(\mathbf{r})$, can be obtained by integrating an appropriate function of the *total* field inside the sphere, $\mathbf{E}(\mathbf{r}')$, over the spherical volume. If we further assume that $\mathbf{E}(\mathbf{r}')$, like the incident field $\mathbf{E}_{\rm inc}(\mathbf{r})$, is perpendicular to the scattering plane, then this integral relationship can be shown (see the Appendix) to be

$$E_s(\mathbf{r}) = \left(\frac{k^2(m^2-1)}{4\pi}\right)\left(\frac{\exp(ikr)}{r}\right)\int_{\rm sphere} E(\mathbf{r}') \times \exp(-ik\hat{s}\cdot\mathbf{r}')dV' , \tag{1}$$

where $\hat{s} = \mathbf{r}/r$.

Equation (1) does not, of course, permit us to calculate the scattered field unless we know the field inside the sphere. We do not know this latter quantity exactly. Nonetheless, if we can make a reasonable estimate of it, Eq. (1) provides us a means of calculating $E_s(\mathbf{r})$. Here, as in the equivalent scattering problem in quantum mechanics, the simplest approximation we can make is to assume that the field at a point inside the sphere is just what it would be if the sphere were not present. This approximation in the quantum mechanical context is just the Born approximation, whereas in this classical electromagnetic problem it is more often referred to as the Rayleigh–Debye (R–D) or Rayleigh–Gans approximation. It is an approximation which is clearly more likely to be valid when m, the relative index of refraction of the sphere, is close to one.

In the R–D approximation, then, we assume the field inside the sphere is given by

$$R(\mathbf{r}') = E_{\rm inc}(\mathbf{r}') = E_0 \exp(ik\hat{s}_0\cdot\mathbf{r}') , \tag{2}$$

where $\hat{s}_0$ is the propagation direction of $E_{\rm inc}(\mathbf{r}')$.

Equations (1) and (2) therefore yield the following expression for $E_s(\mathbf{r})$:

$$E_s(\mathbf{r}) = [k^2(m^2-1)/4\pi]\,[\exp(ikr)/r] \times E_0\int_{\rm sphere}\exp(ik\mathbf{u}\cdot\mathbf{r}')dV' , \tag{3}$$

where $\mathbf{u} = \hat{s}_0 - \hat{s}$. From this definition of $\mathbf{u}$ it follows immediately that $u^2 = 4\sin^2(\theta/2)$. The volume integral in Eq. (3) can be easily evaluated using spherical polar coordinates providing one chooses the z' axis to lie along the vector $\mathbf{u}$. The integral becomes:

$$\int_{\rm sphere}\exp(ik\mathbf{u}\cdot\mathbf{r}')dV' = 2\pi\int_0^a r'^2dr' \times\int_0^\pi \exp(ikur'\cos\theta')\sin\theta'd\theta' . \tag{4}$$

It should be noted that in Eq. (4) θ' is the polar angle (the angle between r' and the z' axis) and is *not* the angle between the incident and scattered radiation. After evaluating the integral we obtain for $E_s(\mathbf{r})$:

$$E_s(\mathbf{r}) = [k^2(m^2-1)]\,[\exp(ikr)/r]a^3E_0J_1(x)/x , \tag{5}$$

where $x = kau = 2ka\sin(\theta/2)$ and $J_1(x) = (\sin x - x\cos x)/x^2$. $J_1(x)$ is often referred to as the first-order spherical Bessel function of the first kind.

At a given distance r from a sphere in free space, the time-averaged value of the intensity of the scattered radiation $I(\theta)$ is equal to $c\epsilon_0|E_s|^2/2$, where c is the velocity of light and ϵ_0 is the permittivity of free space. Thus from Eq. (5) we obtain for $I(\theta)$:

$$I(\theta) = I_0[3J_1(x)/x]^2 , \tag{6}$$

where I_0 is defined by

$$I_0 = c\epsilon_0E_0^2(m^2-1)^2a^6k^4/18r^2 . \tag{7}$$

The quantity $3J_1(x)/x$ approaches one as $x\to 0$. For the special case in which $ka \ll 1$, x will be close to zero for all θ and thus we shall have $I(\theta) = I_0$ for all θ. Let us note that $m^2 = \epsilon/\epsilon_0$, where ϵ is the permittivity of the sphere. If we assume $(m^2-1)\ll 1$, we can write

$$(m^2-1)/3 \simeq (\epsilon-\epsilon_0)/(\epsilon+2\epsilon_0) .$$

Let us also recall that the electric dipole moment of a small linear dielectric sphere in an otherwise uniform electric

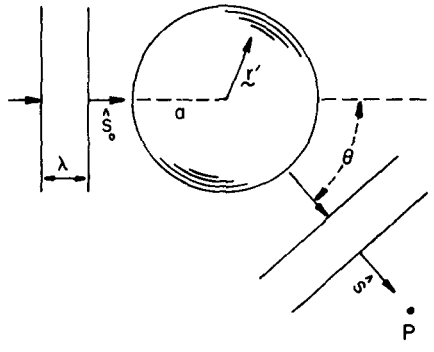

Fig. 1. Scattering geometry. $\hat{s}_0$ and $\hat{s}$ are unit vectors in the incident and scattering directions. $\mathbf{r}'$ is a position vector of a point within the scattering sphere of radius a. P is the point at which the scattered radiation is observed. The position vector of P is $\mathbf{r}$. In the text it is assumed that $r \gg a$.

field E_0 is given by[9]

$$p = 4\pi a^3 \epsilon_0 [(\epsilon - \epsilon_0)/(\epsilon + 2\epsilon_0)] E_0 .$$

Thus for the case of a very small sphere it is reasonable to write Eq. (6) as

$$I(\theta) = I_0 = (cp^2/32\pi^2\epsilon_0 r^2)k^4 . \tag{8}$$

Equation (8) is the standard expression for the time-averaged intensity of the radiation produced by an oscillating dipole in a plane perpendicular to the dipole moment. Equation (8) is, of course, a special case of the famous Rayleigh λ^{-4} scattering.

If ka is not $\ll 1$, then the variation of $I(\theta)$ with θ is determined by the θ dependence of $J_1(x)/x$. This variation, as calculated from Eq. (6), is the R–D approximation of Mie scattering.

Unfortunately, it is easy to demonstrate that the scattering curves obtained from Eq. (6) do not agree with the exact Mie results when ka is comparable to, or greater than, one. Agreement can be improved by using a "modified" R–D approximation. We can, for example, assume that $E(\mathbf{r}')$ is given by Eq. (9) rather than by Eq. (2):

$$E(\mathbf{r}') = E_0 \exp(imk\hat{s}_0 \cdot \mathbf{r}') . \tag{9}$$

In this approximation the field inside the sphere is once again assumed to be a plane wave, but now the phase of the wave depends upon the sphere's index of refraction. With this approximation for $E(\mathbf{r}')$ we can easily demonstrate that $I(\theta)$ is once again given by Eq. (6), where, however, x is now defined by $x = ka(1 + m^2 - 2m\cos\theta)^{1/2}$.

The scattering curves calculated with this "modified" R–D approximation agree somewhat better with the Mie results than do the unmodified R–D results. However, the general shape of any scattering curve obtained from Eq. (6) will depart from the Mie curves because Eq. (6) yields zero for the minimum values of $I(\theta)$, whereas Mie theory does not.

In order to remove these zeros we must alter still further our assumption regarding the field inside the scattering sphere. Let us replace the expression for $E(\mathbf{r}')$ in Eq. (9) by that given in Eq. (10):

$$E(\mathbf{r}') = \mathrm{E}_0[\exp(imk\hat{s}_0 \cdot \mathbf{r}') + \gamma \exp(ik\hat{s} \cdot \mathbf{r}')] . \tag{10}$$

That is, the field inside the sphere is assumed to be a superposition of two plane waves, one traveling in the same direction as the incident wave and the other in the scattering direction. The first term on the right in Eq. (10) is a transmission term which would be present if a plane wave were normally incident upon an infinite plane surface of relative index of refraction m (because we are concerned only with relative scattered intensities, we have arbitrarily set the transmission coefficient equal to one). The second term can be regarded as taking into account the curvature and finite size of the spherically shaped scatterer. If we assume the coefficient γ to be constant as we integrate over the volume of the sphere, we can utilize Eqs. (1), (10), and the definition of $I(\theta)$ to obtain Eq. (11):

$$I(\theta) = I_0[3J_1(x)/x + \gamma]^2 , \tag{11}$$

where again $x = ka(1 + m^2 - 2m\cos\theta)^{1/2}$.

γ is to be regarded as a parameter, the value of which one can vary in order to approximate Mie theory as well as possible. We have tried various numerical values and possible functional forms for γ. We find that for those experimental situations in which we seek to apply the theory, a suitable choice for γ is one in which it has the same sign as

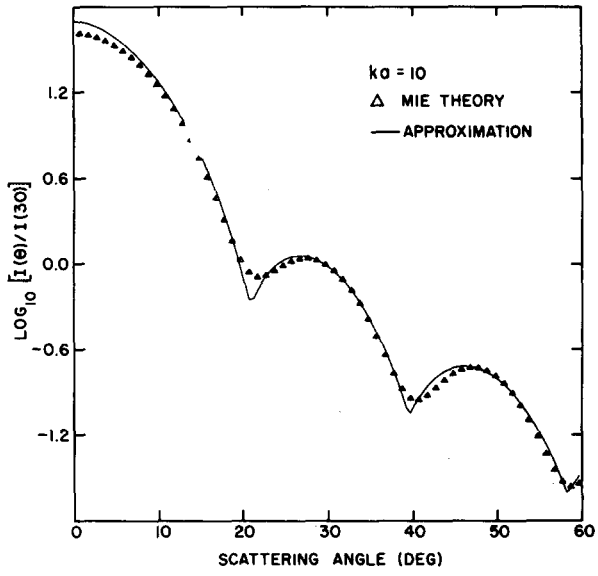

Fig. 2. Scattering pattern of a sphere of circumference-to-incident-wavelength ratio $ka = 10$ and relative index of refraction $m = 1.2$.

$J_1(x)$ and a magnitude which is given by $|\gamma| = x^{-3/2}$.

Up to this point in our discussion we have assumed the incident wave to be polarized perpendicularly to the scattering plane. In Sec. VI, however, we shall describe measurements made with unpolarized light or with light polarized at 45° to the scattering plane. As is discussed elsewhere,[10] for these cases, and for γ defined as in the previous paragraph, Eq. (11) can be replaced by Eq. (12):

$$I(\theta) = I_0(3|J_1(x)|/x + x^{-3/2})^2(1 + \cos^2\theta)/2 , \tag{12}$$

where, as before, $J_1(x) = (\sin x - x\cos x)/x^2$ and $x = ka(1 + m^2 - 2m\cos\theta)^{1/2}$.

In Figs. 2–4 we graph the scattering curves for $m = 1.2$ and $ka = 10$, 15, and 30. The three cases correspond to the scattering of the 0.6328-μm He–Ne laser line by dilute suspensions in water of polystyrene latex spheres of diameters 1.5, 2.25, and 4.5 μm, respectively. For this case

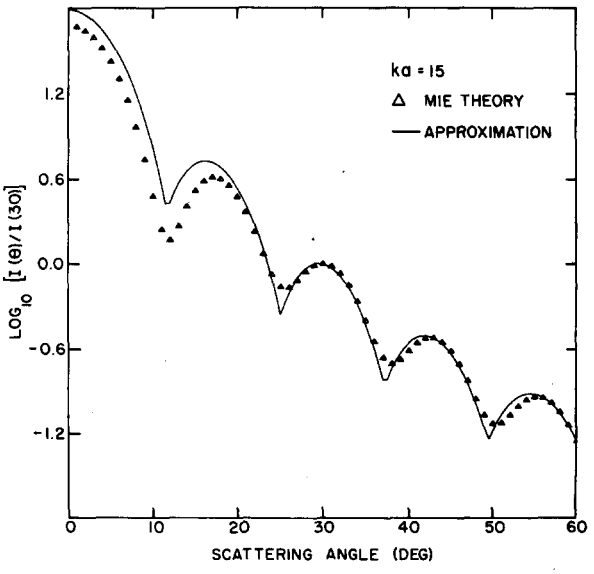

Fig. 3. Scattering pattern for $ka = 15$ and $m = 1.2$.

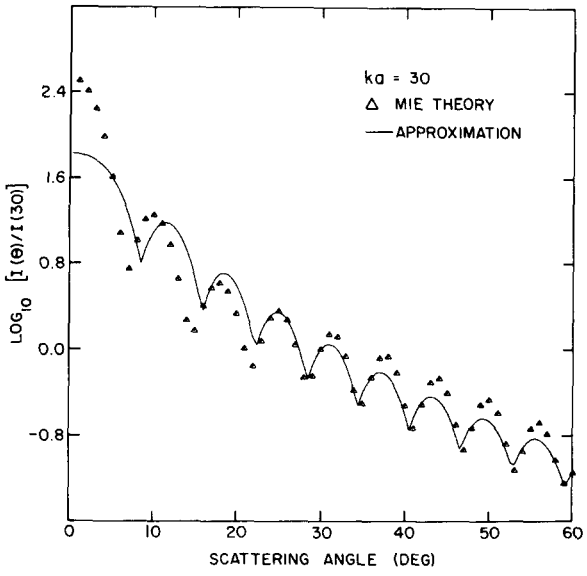

Fig. 4. Scattering pattern for $ka = 30$ and $m = 1.2$.

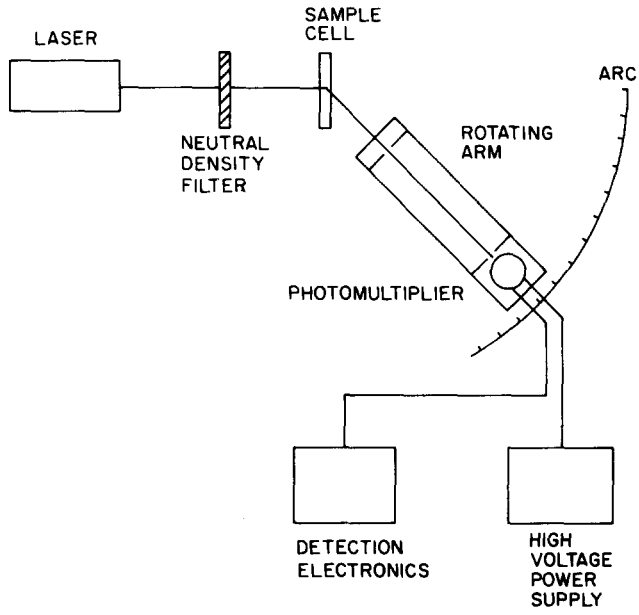

Fig. 5. Block diagram of apparatus used for observing Mie scattering.

$\lambda = 0.6328/1.333\,\mu$m and $m = 1.6/1.333$. In Figs. 2–4 the solid curves are obtained from Eq. (12). The triangles represent the exact Mie results and were obtained using the tables of Chu *et al.*[8] It should be noted that in making measurements, it is relative intensities that we usually wish to compare with theory. It would be most natural to graph $\log[I(\theta)/I(0)]$. However, because the disagreement between the approximate [Eq. (12)] and the exact (Mie) curves is most pronounced at small angles, we have chosen to scale the curves so that all ordinates are zero at the midrange angle $\theta = 30$.

The agreement between the approximate and exact scattering curves is remarkably good in view of the crude approximation we have made for the form of the electric field inside the scattering sphere. Certainly in the case of $ka = 30$, systematic differences between the two curves are evident. Nevertheless, Figs. 2–4 indicate clearly that should we wish to carry out light scattering experiments with polystyrene spheres having ka values in the range 10–30, Eq. (12) will provide us with an easy means of determining whether or not our experimental results are in approximate accord with theory.

III. EXPERIMENT

A block diagram of the apparatus used to observe Mie scattering is shown in Fig. 5. Quite obviously, in this experiment it is necessary to be able to measure the intensity of the scattered laser light as a function of angle. For this purpose we need a movable light detector which has an output that varies linearly (over several decades) with the intensity of light incident upon it. We also need a light source, a sample, and a detecting system which have properties that do not change significantly over the course of the experiment. We shall describe how the various components we used meet these requirements, but we would emphasize at the outset that our choices were often determined by the equipment available to us. Other choices, both of equipment used and of measuring techniques employed, would have served equally well.

Two lasers were used in the experiment: a Coherent model 80 with a power output of 5 mW and a Spectra Physics model 155 which produced 1 mW. Both lasers had more than sufficient power. However, we found that the Coherent laser was more stable. For this reason, all data presented in this article were taken using the Coherent laser, although data taken with the Spectra Physics laser were not qualitatively different. Because of the relatively high power output of the model 80 a neutral density filter with a transmission of 10% was used to reduce the intensity of the beam.

The solution of spheres from which the laser beam was scattered was contained in a rectangular cell. This cell was made by sandwiching a 1-mm-thick plastic spacer with a milled slot between two microscope slides. A thin layer of Apiezon grease coated each side of the spacer, and the entire assembly was held together with spring clamps. The narrow thickness of the sample cell reduced the likelihood of multiple particle scattering and eliminated the need for large quantities of sample. The polystyrene spheres used for this experiment were manufactured by Dow and were obtained from Duke Scientific.[11] The particles had an index of refraction of 1.2 relative to water, and they were suspended in distilled water at concentrations of 0.00075% solids.[11] The solutions of spheres must be sufficiently dilute so that multiple particle scattering is not a predominant effect. That such scattering was negligible was verified by checking that the scattering curves (relative intensities) obtained with samples of different dilutions did not differ markedly. The microscope slides used for the sample cell were first cleaned with a commercial glass cleaner (Micro) and then with very pure acetone. It is very important that the glass be clean and the distilled water be free of contaminants so that the light scattered by the sample holder and water is negligible compared to that scattered by the spheres.

The photomultiplier tube used for this experiment was a Hamamatsu R928 which was mounted in a Thorn EMI RFI/S housing. This tube was originally used for photon correlation work, but it is well suited to this experiment since it has high current gain and low dark noise. The power supply was a Bertan Associates model 215. The appara-

tus was mounted on a pair of 50-cm-long Ealing aluminum triangular optical tracks (model 22-6886). One track was held fixed to the laboratory bench. The second track pivoted about the first. The laser and sample cell were mounted to the fixed track, the latter sitting on a small platform mounted above the pivot. The photomultiplier tube and a set of apertures used to prevent stray light from reaching the tube were mounted on the movable track. Angular positions of the detector were determined with the aid of a large arc (radius = 70 cm) centered on the pivot. We estimate that positions could be reproduced to within $\pm \frac{1}{4}°$. However, the absolute angle of observation may have had an uncertainty as large as $\pm 1°$.

The detection electronics used to monitor the output of the photomultiplier tube (PMT) can be quite simple. It can, for example, be no more than a high-input impedance digital voltmeter. However, the scattered light incident on the PMT, and therefore the PMT's output signal, fluctuate markedly.[12] In order to obtain reasonable scattering curves, it is necessary to average the PMT output, at each angular position, for a time the order of 10–30 s. Under such circumstances, manual data collection and analysis are tedious. We therefore found it desirable, as well as instructive, to incorporate a microcomputer into the detection electronics.

It would be most straightforward to use a good analog-to-digital converter (AD) for reading the PMT output into the computer. However, no suitable AD converter was available to us. We therefore chose a second route. A block diagram of the detection electronics used is shown in Fig. 6. An operational amplifier (Analog Devices 40J) was used to convert the current output of the PMT to a positive voltage, which in turn served as the input to an Analog Devices 452J voltage-to-frequency (VF) converter. The output pulses of the VF converter were counted using a simple 8-bit counting circuit which was read and controlled by a microcomputer and clock. The counter and interface were similar to those described by Miller and Peterson,[13] and were originally used for photon correlation experiments. The clock was a 555 timer configured as a pulse generator.

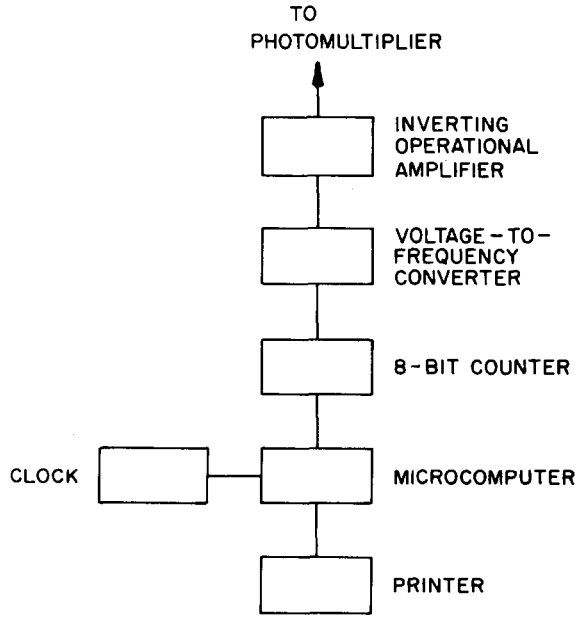

Fig. 6. Block diagram of detection electronics.

Its output was divided down by 2048 with a second counting circuit. When the computer enabled the 8-bit counter, the clock was reset and started. When the most significant bit (the status bit) in the clock's counting circuit went high, it signaled the computer to disable the 8-bit counter.

There are no stringent demands placed upon the microcomputer to be used in this type of experiment. It is our guess that almost any home computer containing a parallel port, several control lines, and several kilobytes of accessible RAM would do. Because it was available to us, we used a Processor Technology SOL 20. The SOL has a parallel port with eight data output and eight data input lines. Several of the former were used as control lines. The external device ready line on the SOL was the status line used by the clock to signal the end of a counting interval.

IV. SOFTWARE

The software used in this experiment had two parts: a BASIC program which handled all user input and printed out the resulting counts, and a machine language program which controlled the counter, and which was called by the BASIC routine. A flow chart for the machine language program is given in Fig. 7. When called, the machine language program first reset and then enabled the counter. It then continually tested the most significant bit of the counter to see if it had changed state. Each time this bit did change state a 16-bit register in the computer was incremented. The program also continually tested to see if the clock had set the status bit. If the status bit was set, the program stopped the 8-bit counter, and saved in memory the current

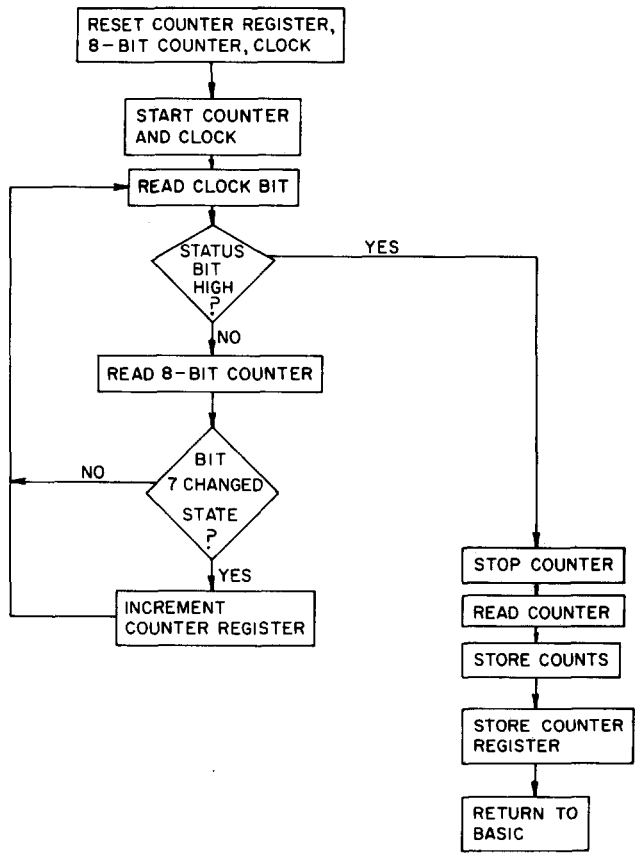

Fig. 7. Flow chart for the machine language program used for controlling and reading the counter.

contents of both the counter and the 16-bit register. Control was then returned to the BASIC program. The accuracy of the counter and software was verified over the entire range of count rates using a Monsanto counter timer.

It should be noted that this method of averaging the PMT output over a time interval determined by the clock circuit has two advantages. First, by testing the most significant bit of the 8-bit counter, we were able easily to record an arbitrarily high number of counts with an 8-bit counter. Second, the method required very little computer memory. Scattering data obtained for a whole set of angular positions could be easily stored.

V. EXPERIMENTAL PROCEDURE

The data were taken every degree between about 10° and 65°. Counting intervals of 20 s were used. Such an interval was long enough to average out fluctuations in the PMT output, but short enough to permit an entire set of data to be taken quickly. Taking the data rapidly reduced variations in the relative intensities due to sedimentation of the sample or drift in the laser's output.

In order to be able to compare experimental and theoretical results, it is, in principle, important to correct the experimental results for background effects. To determine whether background effects were important, we looked at the angular distribution of the light scattered from a sample cell containing only distilled water. Scattering intensities as a function of measured angle for a cell containing distilled water and for one containing a solution of 2-μm-diam spheres are graphed in Fig. 8. As Fig. 8 indicates, background scattering was small compared to the scattering due to the spheres. We therefore ignore background effects in the discussion which follows.

VI. EXPERIMENTAL RESULTS

In Fig. 8 we have graphed scattered intensities versus the observed angular position of the detector. However, in order to compare our data with our theoretical predictions, we must make several corrections. The corrections arise because the scattered radiation, unlike the incident beam, is not normal to air–glass and glass–water interfaces in the sample cell. The scattered radiation is refracted at both surfaces; hence the actual scattering angle θ differs from the observed scattering angle $\theta_{\rm obs}$. The two are related by Eq. (13):

$$\theta = \sin^{-1}(n^{-1}\sin\theta_{\rm obs}), \tag{13}$$

where n is the index of refraction of water relative to air. Because these two angles differ, we must correct not only the observed scattering angles, but also the observed scattering intensities. Corrections to the latter must be made for two reasons. First, since $d\theta_{\rm obs}/d\theta$ is not constant, the effective solid angle intercepted by the detector changes with θ. A second correction must be made to account for the fact that the fraction of scattered radiation which is transmitted at each interface also varies with angle.

In Figs. 9 and 10 we graph the corrected scattering data for 0.6328-μm light scattered from two sizes of polystyrene latex spheres. Although in the experiments the maximum value of $\theta_{\rm obs}$ was 65°, Eq. (13) makes it clear that the maximum value of θ will be $\sim$43°. The spheres used had diameters of 2 and 5 μm. Thus the relevant values of the parameter ka are 13.3 and 33, respectively. The former value is bracketed by 10 and 15 and the latter is reasonably close to 30. A comparison of the approximate and exact Mie scattering curves shown in Figs. 2–4 indicates that approximate scattering curves calculated for $ka = 13.3$ and 33 should provide an adequate test of our experimental measurements. Thus in Figs. 9 and 10 the solid curves are calculated from Eq. (12) and the circles represent the experimental results. For both theory and experiment we scale the curves so that they will overlap at $\theta = 22°$. This value has been chosen since it lies close to a maximum for both ka values, and since Figs. 2–4 indicate that our approximate scattering curves fit Mie theory better in the vicinity of maxima than near the minima.

Agreement between the experimental and theoretical results is comparable to that reported elsewhere.[14] It is evident from Figs. 9 and 10 that the measured and theoretical

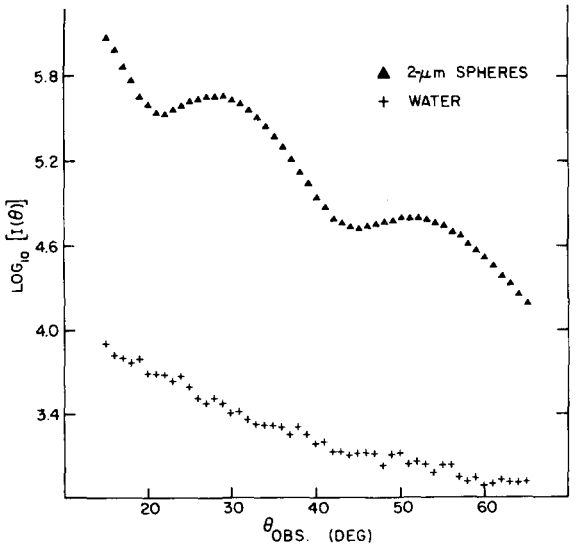

Fig. 8. Scattering from a suspension of 2-μm spheres (triangles) and from distilled water (crosses). The ordinate is the logarithm of the number of counts in a 20-s interval. $\theta_{\rm obs}$ is the angle between the detector and the direction of the incident laser beam. The difference between $\theta_{\rm obs}$ and the actual scattering angle is discussed in the text.

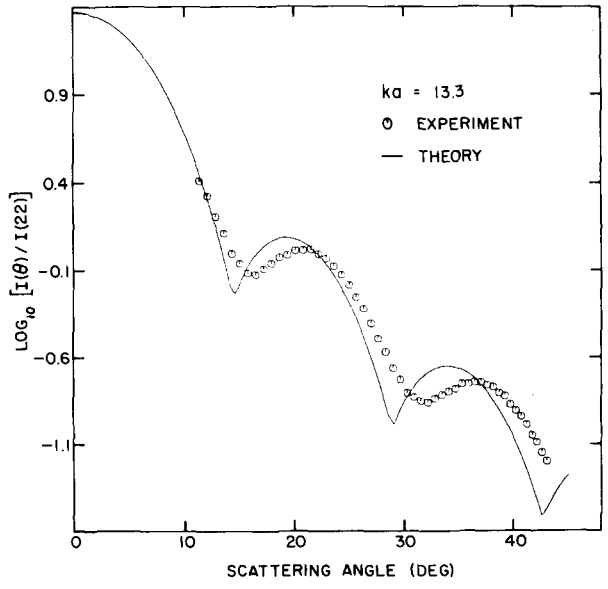

Fig. 9. Scattering pattern for $ka = 13.3$ (2-μm spheres).

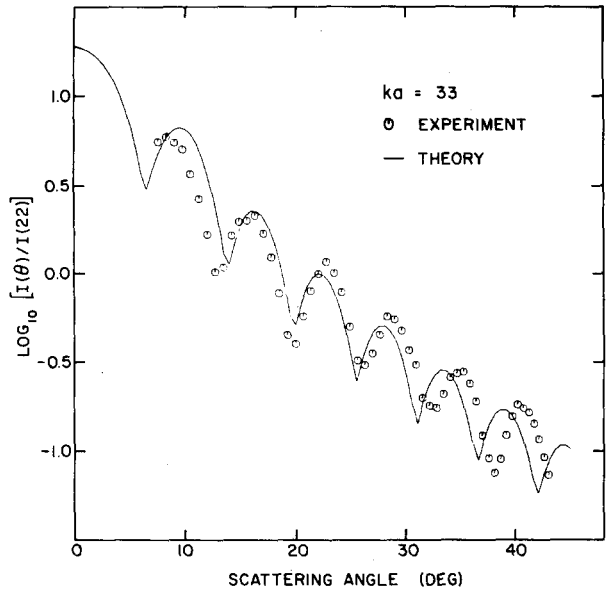

Fig. 10. Scattering pattern for $ka = 33$ (5-μm spheres).

angular positions of the extrema do not always coincide, but a glance at Figs. 2–4 indicate that at least some portion of this discrepancy arises from the fact that our approximation of Mie theory is, after all, only approximate. A comparison of Figs. 4 and 10, for example, shows that in both figures the extrema in the approximate curve come at larger angles for small θ and at smaller angles for large θ than do the extrema for either Mie theory or the experimental results. We can be certain then, that were we to carry out the exact Mie calculation for the case $ka = 33$, the agreement between experiment and (exact) theory would be better than that shown in Fig. 10.

VII. SUMMARY

We have presented an analytical method for approximating Mie theory. The method enables one to calculate easily the angular variation of light scattered by a dilute suspension of latex spheres, and thereby to compare experimental and theoretical results. We have also described an apparatus for measuring the scattering of the 0.6328-μm He–Ne line from 2- and 5-μm-diam polystyrene latex spheres, and have found the agreement between theory and experiment to be reasonably good. Light scattering has been, and continues to be, of both theoretical and experimental interest to physicists. We hope the techniques described here show this subject to be accessible to the advanced undergraduate.

APPENDIX

In the Mie scattering problem we have a plane wave, $\mathbf{E}_{\rm inc}(\mathbf{r},t) = \mathbf{E}_0 \exp[i(k\hat{s}\cdot\mathbf{r} - \omega t)] = \mathbf{E}_{\rm inc}(\mathbf{r})\exp(-i\omega t)$, incident upon a small sphere which is centered at $\mathbf{r} = 0$ and which has a relative index of refraction m. Initially we shall allow the possibility that m varies with $\mathbf{r}$. We assume both the sphere and the region outside to be nonmagnetic and to have no free currents or charges. If the total field at $\mathbf{r}$ can be written $\mathbf{E}(\mathbf{r},t) = \mathbf{E}(\mathbf{r})\exp(-i\omega t)$, then it follows from Maxwell's equations that $\mathbf{E}(\mathbf{r})$ must satisfy

$$\nabla^2\mathbf{E} + k^2\mathbf{E} = -k^2(m^2-1)\mathbf{E} + \nabla\{\nabla\cdot[(m^2-1)\mathbf{E}]\}\,. \tag{A1}$$

However, $\mathbf{E}(\mathbf{r}) = \mathbf{E}_s(\mathbf{r}) + \mathbf{E}_{\rm inc}(\mathbf{r})$, where $\mathbf{E}_s(\mathbf{r})$ is the spatial part of the scattered field at $\mathbf{r}$. Since $\nabla^2\mathbf{E}_{\rm inc} + k^2\mathbf{E}_{\rm inc} = 0$, Eq. (A1) becomes

$$\nabla^2\mathbf{E}_s + k^2\mathbf{E}_s = \mathbf{H}(\mathbf{r})\,, \tag{A2}$$

where $\mathbf{H}(\mathbf{r})$ is defined by the right-hand side of Eq. (A1).

Let us denote one component of $\mathbf{E}_s(\mathbf{r})$ by $e(\mathbf{r})$ and the corresponding component of $\mathbf{H}(\mathbf{r})$ by $h(\mathbf{r})$. Then

$$\nabla^2 e + k^2 e = h(\mathbf{r})\,. \tag{A3}$$

Mott and Massey[15] show that for this problem $e(\mathbf{r})$ is given by

$$e(\mathbf{r}) = \left(\frac{-1}{4\pi}\right)\int_{\rm sphere}\left(\exp\frac{(ikR)}{R}\right)h(\mathbf{r}')dV'\,, \tag{A4}$$

where $R = |\mathbf{r} - \mathbf{r}'|$, and the prime indicates integration over the sphere. If $r \gg r'$ then Eq. (A4) becomes, since $\hat{s}$ is parallel to $\mathbf{r}$,

$$e(\mathbf{r}) = \left(\exp\frac{(ikr)}{r}\right)\left(\frac{-1}{4\pi}\right)\int_{\rm sphere}\exp(-ik\hat{s}\cdot\mathbf{r}')h(\mathbf{r}')dV'\,. \tag{A5}$$

Since Eq. (A5) holds for each component of $\mathbf{E}_s(\mathbf{r})$ and $\mathbf{H}(\mathbf{r})$, we can, remembering the definition of $\mathbf{H}(\mathbf{r})$, write

$$\mathbf{E}_s = \left(\exp\frac{(ikr)}{r}\right)\left(\frac{-1}{4\pi}\right)\int_{\rm sphere}\exp(-ik\hat{s}\cdot\mathbf{r}') \times\{-k^2(m^2-1)\mathbf{E} + \nabla'[\nabla'\cdot(m^2-1)\mathbf{E}]\}dV'\,. \tag{A6}$$

In Eq. (A6) we have used the definition of $\mathbf{H}(\mathbf{r})$ appropriate to the region inside the sphere. For the case of a homogeneous sphere m = constant, and the only contribution from the second term is that which arises from the discontinuity in m at the surface of the sphere. It is possible to show that for this case Eq. (A5) becomes

$$\mathbf{E}_s(\mathbf{r}) = [\exp(ikr)/r][k^2(m^2-1)/4\pi] \times\int_{\rm sphere}\{\mathbf{E}(\mathbf{r}') - [\mathbf{E}(\mathbf{r}')\cdot\hat{s}]\hat{s}\}\exp(-ik\hat{s}\cdot\mathbf{r}')dV'\,. \tag{A7}$$

For the special case in which $\mathbf{E}_{\rm inc}$ is perpendicular to the scattering plane and $\mathbf{E}$ is assumed to be parallel to $\mathbf{E}_{\rm inc}$, Eq. (A7) reduces to Eq. (1).

ACKNOWLEDGMENTS

We are grateful to M. R. Peterson for suggesting the design of the sample cell, and to K. Jagannathan for many helpful discussions regarding scattering theory.

[a] Apparatus design and experimental results are described in greater detail in the senior honors thesis submitted by RMD in partial fulfillment of the Senior Honors Research Program at Amherst College.

[1] Lord Rayleigh, Philos. Mag. **41**, 447 (1871).
[2] Lord Rayleigh, Proc. Math. Soc. (London) **4**, 253 (1872).
[3] G. Mie, Ann. d. Phys. **25**, 377 (1908).
[4] M. Kerker, *The Scattering of Light and Other Electromagnetic Radiation* (Academic, New York, 1969).
[5] N. A. Logan, Proc. IEEE **53**, 773 (1965).
[6] L. E. Ashley and C. M. Cobb, J. Opt. Soc. Am. **48**, 261 (1958).
[7] H. H. Denman, W. Heller, and W. J. Pangonis, *Angular Scattering Functions for Spheres* (Wayne State U.P., Michigan, 1966).
[8] C. M. Chu, G. C. Clark, and S. W. Churchill, *Tables of Angular Distribution Coefficients for Light Scattering by Spheres* (Eng. Res. Inst., Univ. of Michigan, Ann Arbor, MI, 1957).

[9]D. J. Griffiths, *Introduction to Electrodynamics* (Prentice Hall, Englewood Cliffs, NJ, 1981), p. 162.
[10]J. E. Gordon, J. Opt. Soc. Am. A **2**, 156 (1985).
[11]Duke Scientific Corp, 445 Sherman Ave., Palo Alto, CA 94306. The solutions obtained from Duke had concentrations of 0.1% solid. These solutions were then diluted by a factor of 133 with distilled water.
[12]N. A. Clark, J. H. Lunacek, and G. B. Benedek, Am. J. Phys. **38**, 575 (1970).
[13]S. R. Miller and M. A. Peterson, Am. J. Phys. **50**, 1129 (1982).
[14]F. T. Arecchi, M. Giglio, and U. Tartari, Phys. Rev. **163**, 186 (1967).
[15]N. F. Mott and H. S. W. Massey, *The Theory of Atomic Collisions* (Oxford U.P. London, 1965), 3rd ed., pp. 76–80.

A push-me–pull-you water-driven wheeled vehicle

A. Rubčić and J. Baturić-Rubčić
Department of Physics, Faculty of Science, P. O. Box 162, Zagreb, Yugoslavia

(Received 6 September 1983; accepted for publication 30 September 1984)

A model rail vehicle driven by a flow of water has been constructed and investigated. Instead of railway sleepers, a channel with a water stream running between the rails is required. The "engine" of the vehicle is an ordinary water wheel, which draws energy from the water. Both upstream and downstream motions are possible. Theoretical and experimental characteristics of the vehicle are demonstrated.

I. INTRODUCTION

Recently, Blackford wrote on the physics of a push-me–pull-you boat[1] and a wind-driven wheeled vehicle[2] which includes wind-to-water and wind-to-ground interactions. This leaves the consideration of water-to-ground interaction. For that purpose we constructed a "stern-wheeler" model which moves on rails. A water wheel was mounted on the rear shaft of the vehicle, whose four "ground wheels" can roll along the rails. The paddles of the water wheel were immersed in a flow of water running along a channel below the vehicle and between the rails. A sketch of the rail vehicle with a water wheel acting as its "engine" is shown in Fig. 1.

Usually, a water wheel is used in a water mill or, with various modifications, in a turbine, to draw a certain amount of energy from the flow of water. Such devices are stationary ones. The vehicle of our design allows a translational degree of freedom to the water wheel along the water stream. In other words, the vehicle may be regarded as a movable water mill, just as Blackford's wind vehicle[2] might be understood analogously as a movable windmill.

II. THEORY

A. Stationary water wheel

The force of the water flow on the paddle of the stationary water wheel can be deduced easily. One has to start with elementary physical laws of motion, mass, and momentum conservation and Bernoulli's theorem.[1] A constant mass in a flow along stream lines leads to equalities

$$A_1 v_1 = A_2 v_2 = A_3 v_3, \tag{1}$$

where A_1 and A_3 are cross-sectional areas of the chosen stream tube far upstream and far downstream of a stationary wheel, respectively. The associated velocities are: v_1, the initial undisturbed velocity in front of the water wheel; v_2, generally diminished velocity in area A_2 of the paddle from which power is supplied to the water wheel; and velocity v_3, far downstream of the water wheel (denoted hereafter by ww).

The difference between input rate of momentum and output rate of momentum of the water flow must be equal to the force of water on the paddle, due to momentum conservation, i.e.,

$$F_w = \rho(A_1 v_1^2 - A_3 v_3^2), \tag{2}$$

where ρ is water density. Bernoulli's theorem may now be used to express velocity v_3 by means of v_1 and v_2. Applying this theorem to the input and output sides of the ww, we obtain two equations in the following form:

$$P_i + \tfrac{1}{2}\rho v_i^2 = P_{2j} + \tfrac{1}{2}\rho v_2^2,$$

where $i = 1,3$ and $j = u,d$. P_1 and P_{2u}, and P_3 and P_{2d} are associated pressures far and immediately upstream and downstream, respectively. Thus with $P_1 = P_3 = P_0$, change of pressure just on the paddle is

$$\Delta P = P_{2u} - P_{2d} = \tfrac{1}{2}\rho(v_1^2 - v_3^2),$$

resulting in the force on the paddle $F_w = A_2 \Delta P = \rho A_2(v_1^2 - v_3^2)/2$. From this relation and by means of Eqs. (1) and (2) it follows rather straightforwardly that $v_3 = v_1(2v_2/v_1 - 1)$. Thus force F_w may be expressed by

$$F_w = 2\rho A_2 v_2(v_1 - v_2). \tag{3}$$

Finally, the power drawn from the water by the paddle is

$$P_w = F_w v_2 = 2\rho A_2(v_1 - v_2)v_2^2. \tag{4}$$

Taking $v_2 = v_1(1 - a)$, where $0 < a < 1$, Eqs. (3) and (4) are identical to Eqs. (6) and (7) in Ref. 1, obtained for a windmill with a propeller with a constant swept area A_2.

However, our ww model (Fig. 1) has a narrow channel for water flow which only slightly exceeds the width of the paddles of the ww. Therefore, at higher velocity ratio v_1/v_2,

